JSS Focus Issue on Semiconductor-Based Sensors

ZnO Nanowall Networks for Sensor Devices: From Hydrothermal Synthesis to Device Demonstration

Zixuan Feng,[1] Subrina Rafique,[1,2] Yi Cai,[2] Lu Han,[2] Ming-Chun Huang,[2] and Hongping Zhao [1,2,3,*,z]

[1] *Department of Electrical and Computer Engineering, The Ohio State University, Columbus, Ohio 43210, USA*
[2] *Department of Electrical Engineering and Computer Science, Case Western Reserve University, Cleveland, Ohio 44106, USA*
[3] *Department of Materials Science and Engineering, The Ohio State University, Columbus, Ohio 43210, USA*

This paper reports the synthesis of ZnO nanowalls (NWLs) on various substrates by low cost and scalable hydrothermal approach targeting for flexible sensor device applications. Prototype flexible piezoelectric sensor devices using the synthesized ZnO NWLs were demonstrated through a transfer process. The roles of precursor chemical concentration and aluminum seed layer thickness in determining the morphology and the growth rate of the as grown ZnO NWLs were investigated. Effects of thermal annealing on the morphology and the crystalline quality of the NWLs were studied. To fabricate the sensor devices, ZnO NWL layers were transferred on to different substrates using thin Polymethyl methacrylate (PMMA) layer. Wafer scale transfer of thermally annealed ZnO NWLs to flexible substrates has been achieved. The demonstrated prototype devices can generate up to 300 mV of output voltage with external applied forces. Simulation model using COMSOL Multiphysics was developed to study the piezoelectric properties of the ZnO NWLs based devices. The simulation results agree well with the experimental data. The demonstrated ZnO NWLs based flexible devices are applicable for wearable nanodevices and motion sensors that will benefit from their large surface areas.
 [DOI: 10.1149/2.0221807jss]

Manuscript submitted January 30, 2018; revised manuscript received March 27, 2018. Published April 14, 2018. *This paper is part of the JSS Focus Issue on Semiconductor-Based Sensors for Application to Vapors, Chemicals, Biological Species, and Medical Diagnosis*.

Recently, wearable electronics have become one of the trending technologies for their potential applications in personal fitness, medical care and communication. A compact, flexible and sustainable piezoelectric device can play important roles in wearable electronics such as: (i) energy harvesting, which converts mechanical energy into electricity and powers up devices; (ii) pressure sensors, which detect forces and transform them into electrical signals for further analysis.

Semiconductor material ZnO possesses a large bandgap of ~3.37 eV, a large exciton binding energy of 60 meV[1] and decent piezoelectric properties. Because of such unique properties, ZnO is a promising candidate for various device applications such as sensors/biosensors, photodetectors/solar cells, resistive random-access memory and surface acoustic wave devices.[2–7] As a result, considerable efforts are going on to synthesize ZnO based nanostructures with one-dimensional (1D) and two-dimensional (2D) morphologies such as nanowires,[8–10] nanorods,[1,11,12] nanowalls[13–15] and nanobelts[16–18] by various growth techniques. ZnO nanostructures have become the focus of intensive research due to their applicability in nanoscale devices. ZnO nanowalls (NWLs) are featured with interconnected honeycomb-like structure with large surface-to-volume ratio, and good mechanical durability. Due to its planar structure, the traditional top-down fabrication process is still applicable. Material synthesis processes such as chemical vapor deposition (CVD), metal organic chemical vapor deposition (MOCVD), and molecular beam epitaxy (MBE) require expensive apparatus and processes which are time consuming and typically conducted at elevated temperatures. On the other hand, solution based synthesis process is low cost and scalable. It yields high throughput at much lower operating temperatures. Consequently, numerous studies have been published in the literature on the synthesis of ZnO thin films,[19] nanorods,[20–22] nanowires[23–25] and nanowalls[26–28] using hydrothermal synthesis process.

Mechanical transfer process for thin films has been developed with graphene, and other 2D materials, proving flexibility for multiple application purposes.[29–31] The polymethyl methacrylate (PMMA)-mediated transfer method is one of the common transfer techniques. With this transfer method, there are fewer restrictions on substrate and contact selection which allows a wide range of device designs.[32] Devices based on transferred ZnO nanostructures have been reported previously for field effect transistors,[33] strain sensors[34] and nanogenerators.[35] In this paper, we demonstrated flexible ZnO nanowalls based piezoelectric device fabrication using the combination of hydrothermal synthesis and mechanical transfer of thermally annealed ZnO NWLs. Here, we have developed a process that allows to achieve wafer scale transfer of high crystalline quality ZnO NWLs to flexible substrates through (i) hydrothermal synthesis of large area and uniform ZnO NWLs; (ii) thermal annealing of ZnO NWLs; and (iii) wafer scale mechanical transfer of ZnO NWLs by using PMMA. The process was optimized by considering the trade-off between the thermal annealing temperature and feasibility of mechanical transfer. The maximum output voltage from the fabricated sensor devices is around 300 mV, which is comparable with the similar devices reported in the literature.[35–37]

Experimental

Synthesis of ZnO NWLs.—Figure 1 shows the schematic of the ZnO NWLs growth procedure. SiO_2-on-Si, Si, polyimide (PI) and polyethylene terephthalate (PET) were used as the growth substrates. Prior to the growth, the substrates were cleaned with acetone and isopropanol, rinsed by deionized water and dried with nitrogen flow. Aluminum (Al) seed layer with different thicknesses (100 nm, 200 nm) were deposited on the substrates via thermal evaporation. The ZnO

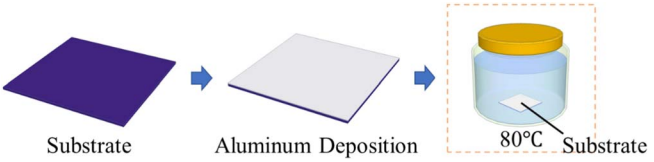

Figure 1. Schematic diagram of the setup for ZnO NWL hydrothermal synthesis.

*Electrochemical Society Member.
[z]E-mail: zhao.2592@osu.edu

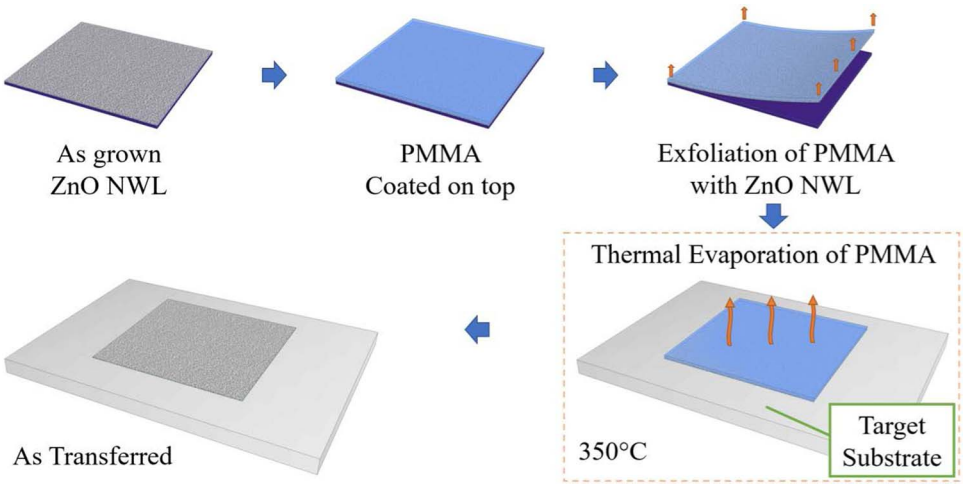

Figure 2. Schematic diagram of the mechanical transfer process for ZnO NWL.

NWLs were grown in an aqueous solution of zinc nitrate hexahydrate (ZNH, $Zn(NO_3)_2 \cdot 6H_2O$) and hexamethylenetetramine (HMT, $(CH_2) \cdot 6N_4$) at 80°C for 30 minutes. To study the effects of the chemical concentration on the morphology of the synthesized ZnO NWLs, several experiments were conducted using different molar ratios of ZNH and HMT (2:1, 1:1 and 1:2). For these experiments, a constant ZNH concentration of 25 mM was used with the total solution volume of 40 mL. After finishing the growth, the samples were removed from the solution, rinsed with DI water and dried with nitrogen. The effects of thermal annealing at elevated temperatures ($T_{annealing} = 350°C$, 600°C, 800°C) for 3 hrs on the ZnO NWLs surface morphology and crystalline quality were also investigated.

Mechanical transfer.—The mechanical transfer process of the ZnO NWLs is illustrated in Fig. 2. PMMA solution (anisole as solvent, 7% concentration, MicroChem) was drop-coated on top of the grown sample and deposited uniformly by film applicator. Then the sample was dried on hot plate for 1 hr at 60°C. Using a blade, the PMMA film with ZnO NWLs attached was exfoliated from the growth substrate. The film was then embedded between two glass slides and put on hot plate for 2 hrs at 90°C. Heat curing of the film helped to release the strain and maintained the flatness of the PMMA film. After curing, the film was released from the glass slides and placed on the designated area of the target substrate. The film was hold in place on the substrate by anchoring its corners, protecting itself from disturbance in air. Furnace was then used to heat up and evaporate PMMA (350°C, 2 hrs) and left ZnO NWLs on the target substrate. The post-transferred ZnO NWLs were characterized by optical imaging and FESEM to demonstrate the integrity and effectiveness of the transfer process.

Piezoelectric device design and fabrication.—Figure 3 shows the schematic of the prototype device. Polyimide (PI, HPP-ST 2mil, DuPont) served as both top and bottom substrates and Ti/Au was deposited as contact. The size of the central contact area is 1 cm × 1 cm. Au stripe of 3 mm wide is extended to one side of the substrate to serve as the contact pad for wirings. The ZnO NWL films were transferred to the bottom PI substrate and then packed with top substrate. The areas of the transferred films were larger (1.5 cm × 1.5 cm) as compared to those of the Au contact pads, avoiding crosstalk between top and bottom contacts after transfer. Epoxy adhesive (Poxy Pak, Henkel) was applied on the edges of PI substrates for device packaging. Copper wires were connected to the outer contact pads to form extended connection. To confirm the sources of the voltage pulses, we also fabricated one reference device with no ZnO NWLs embedded in between the PI substrates. Numerical simulation was also conducted using COMSOL Multiphysics to study the piezoelectric properties of the ZnO NWLs.

Characterization.—The morphology, crystalline quality and optical properties of the ZnO NWLs were characterized by using field emission scanning electron microscopy (FESEM), scanning electron microscopy (SEM), X-ray diffraction (XRD) and photoluminescence (PL) spectroscopy. FESEM images were taken with Helios 650. The SEM images were taken with Tescan Vega-3. XRD spectra were collected on a Bruker Discover D8 X-Ray Diffractometer with Cu Kα radiation (1.54 Å). PL spectra were measured at room temperature using a Jobin Yvon-spex-Fluorog-3-Spectrofluorimeter with a 450 W Xenon lamp as the light source. Piezoelectric voltage measurement was logged by Tektronic TPS 2024B Oscilloscope and retrieved through RS-232 port.

Results and Discussion

To study the effects of HMT molar concentration on the morphology of the synthesized ZnO NWLs, syntheses were conducted at 80°C for 30 mins. For all the experiments, the ZNH concentration was fixed at 25 mM while varying the HMT concentration in the range between 12.5 mM and 50 mM. Figure 4 shows the top view SEM images of the as-grown ZnO NWLs on SiO_2-on-Si substrate covered with 100 nm Al film using different HMT concentrations. For HMT concentrations of 25 mM and 12.5 mM (Fig. 4a and Fig. 4b), the morphologies of the ZnO NWLs are similar. As the concentration of the HMT increases to 50 mM, the synthesis process resulted in the formation of flower-like ZnO nanoparticles on top of the NWLs networks. Tang. et al. observed the similar phenomenon previously.[38] The higher concentration of HMT provides more $Zn(OH)_4^{2-}$ ions (Eqs. 1–3) in

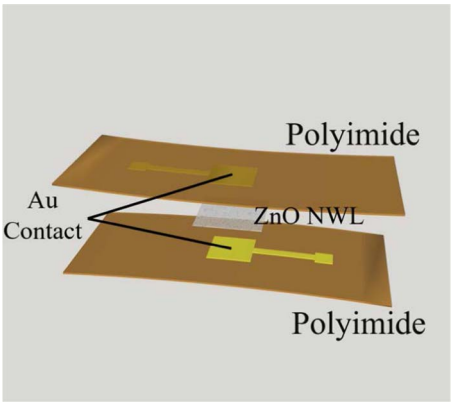

Figure 3. Schematic diagram of the prototype ZnO NWL piezoelectric device.

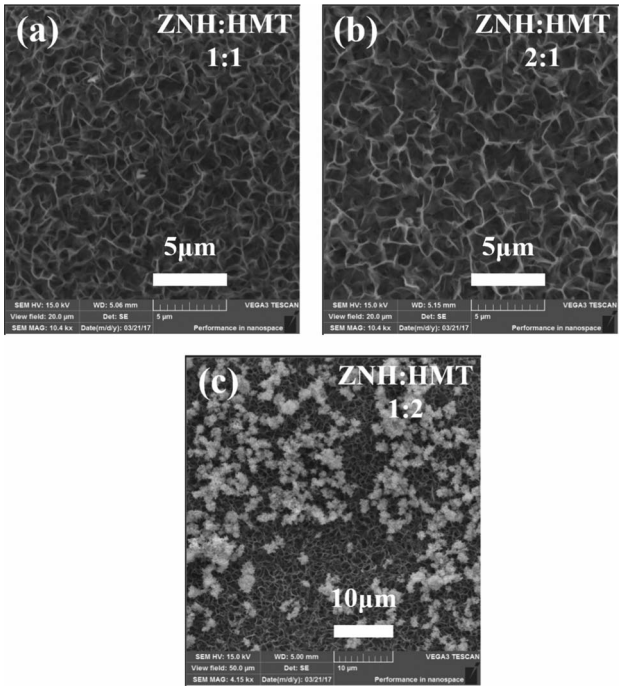

Figure 4. Top view SEM images of ZnO NWLs grown at 80°C on SiO_2/Si substrate with three different ZNH: HMT molar ratios: (a) 1:1; (b) 2:1; and (c) 1:2.

the solution which leads to the fast nucleation of ZnO crystallites in different crystal orientations such as [10-10] orientation,[39,40] which promotes the formation of nanoflowers. From this study, we determined the optimum chemical concentration of ZNH and HMT (1:1) for later solution synthesis.

$$(CH_2)_6N_4 + H_2O \rightarrow HCHO + NH_3 \quad [1]$$

$$NH_3 + H_2O \rightarrow NH_4^+ + OH^- \quad [2]$$

$$Zn^{2+} + OH^- \rightarrow Zn(OH)_4^{2-} \rightarrow ZnO \quad [3]$$

To investigate the effects of Al seed layer thickness on the growth rate, cross sectional SEM was conducted. It is known that the use of Al seed layer is critical to promote the formation of NWL structure instead of nanorod structure.[41–43] Al oxidizes in the solution and forms AlO_2^- (Eq. 4). The binding of AlO_2^- to the Zn^{2+} terminated surface suppresses the growth of ZnO along the [0001] polar orientation and thus promotes its growth in the lateral orientation.[41,42]

$$Al^{3+} + OH^- \rightarrow Al(OH)_3 + OH^- \rightarrow AlO_2^- \quad [4]$$

Figure 5 shows the cross-sectional SEM images of the ZnO NWLs grown on SiO_2-on-Si substrate with different Al thicknesses using the same concentration of ZNH and HMT (molar ratio = 1:1). The growths were conducted for 30 mins. The ZnO NWLs grown on the 100 nm thick Al layer had a thickness of ~1.6 µm, which corresponds to a growth rate of ~3.2 µm/hr. On the other hand, the ZnO NWLs grown on 200 nm thick Al layer had a thickness of ~3.3 µm which corresponds to a growth rate of ~6.4 µm/hr. Our studies indicate that the ZnO NWLs growth rate increases with the increase of the seed layer thickness, due to the increase of the AlO_2^- concentration in the solution.[43] However, for both cases, the formation of the nanoparticles on top of the NWLs occurs with longer growth time. This indicates the shift of growth kinetic from the formation of nanowalls to nanoflowers due to the decrease of AlO_2^- concentration while the precipitation of ZnO is still fast. This is due to the screening of Al film by NWLs as it grows.

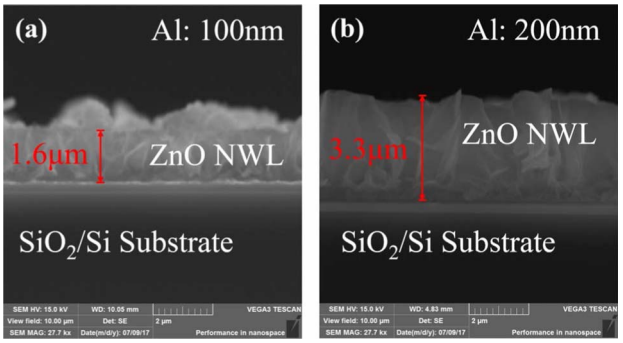

Figure 5. Cross sectional SEM images of ZnO NWLs grown at 80°C on SiO_2/Si substrate with ZNH: HMT molar ratio of 1:1 using different Al film thicknesses: (a) 100 nm; and (b) 200 nm.

To study the effects of the growth substrate on the ZnO NWLs morphology, we synthesized ZnO NWLs on different substrates: SiO_2-on-Si (SiO_2/Si), Si (100), Si (111), PET and PI. The growth was conducted at 80°C for 30 mins using 1:1 molar ratio of ZNH and HMT. The Al seed layer thickness was 100 nm. The surface morphologies of the as-synthesized ZnO NWLs on different substrates are similar. This indicates the flexibility of the substrate selection for the hydrothermal synthesis of ZnO NWLs for various applications.

Due to the large defect concentration in hydrothermal synthesized ZnO materials, thermal annealing process is typically utilized to improve the crystalline quality of the material, thus to improve the piezoelectric properties of the material for sensor device application.[36] To study the effects of thermal annealing on the surface morphology, crystalline quality and optical properties of the synthesized ZnO NWLs, several annealing experiments were conducted at different temperatures (350°C, 600°C and 800°C). All the experiments were conducted under the flow of oxygen and argon for 3 hrs. Figure 6 shows the top view SEM images of the as-grown and annealed ZnO NWLs with different annealing temperatures. As can be seen from the images, ZnO NWL structure regresses with increased annealing temperature. This indicates the ZnO NWLs tends to agglomerate during high temperature annealing process.

Figure 7 plots the XRD spectra of the as-grown ZnO NWLs as compared to the materials after annealing at different temperatures. The as grown and annealed ZnO NWLs show polycrystalline properties with wurtzite ZnO structure. For all the spectra, ZnO (110), (200) and (201) peaks are clearly visible (JCPDS#80-0074). After thermal

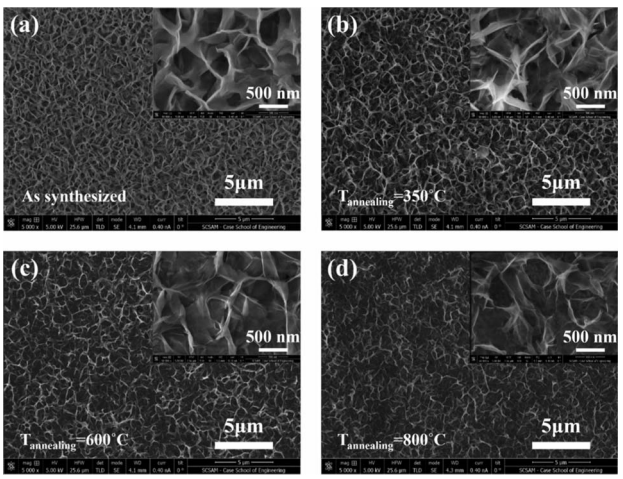

Figure 6. Top view FESEM images of ZnO NWLs annealed at different temperatures; (a) as synthesized, (b) $T_{annealing}$ = 350°C, (c) $T_{annealing}$ = 600°C, and (d) $T_{annealing}$ = 800°C.

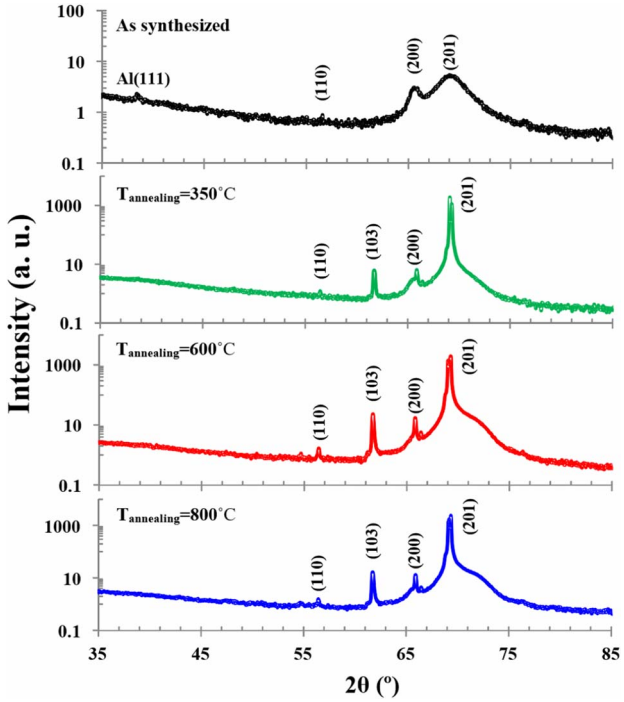

Figure 7. XRD spectra (θ-2θ scan) of ZnO NWLs: as synthesized vs. annealing at different temperatures: $T_{annealing} = 350°C$, $T_{annealing} = 600°C$ and $T_{annealing} = 800°C$.

annealing, ZnO (103) peak appeared, and the NWLs exhibited sharp (201) peak with higher intensity. The intensities of the (110), (103), and (200) peaks also increased with increasing annealing temperature. This indicates that high-temperature thermal annealing can improve the crystalline quality of the ZnO NWLs.

Figure 8 shows the PL spectra of the as-grown and annealed ZnO NWLs. The NWLs exhibited near band edge emission at ~380 nm and broad deep level emission around 540–580 nm. As the annealing temperature increases, the overall intensity of the spectrum decreases, which is partially due to the reduced NWL thickness as NWLs agglomerate. Note that the intensity of the green luminescence reduces significantly as the annealing temperature increases. It has been reported previously that the green emission is related to the oxygen vacancies (V_O) in ZnO.[44,45] The relatively high intensity of the green emission peak in the as-grown ZnO NWLs is due to the strong bonding

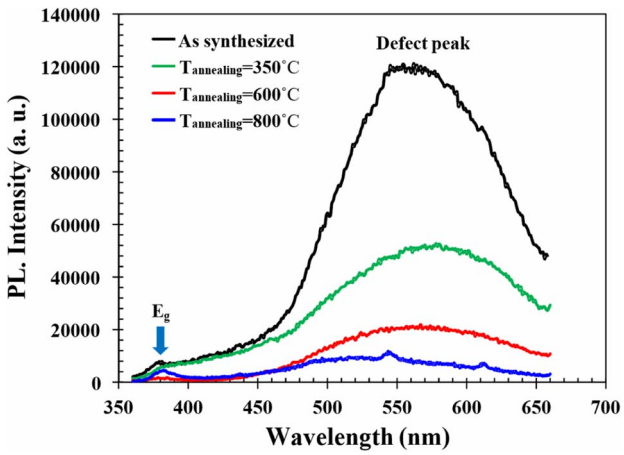

Figure 8. Room temperature PL spectra of ZnO NWLs: as synthesized vs. annealing at different temperatures: $T_{annealing} = 350°C$, $T_{annealing} = 600°C$ and $T_{annealing} = 800°C$.

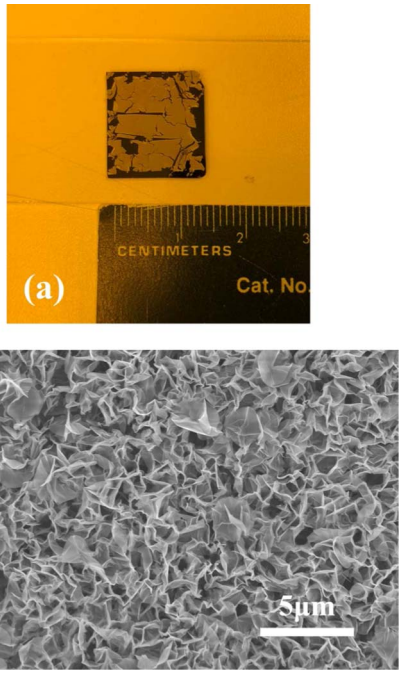

Figure 9. Transferred ZnO NWLs on Si substrate. (a) Photo image; and (b) Top view SEM image of the film.

between Al and O[46] leading to high density of V_O. With the thermal annealing under oxygen atmosphere, the reduction of V_O contributed to the reduction of the intensity of green emission peak.

From our systematic studies, we identified the optimal synthesis condition of ZnO NWLs (ZNH: HMT = 1:1) and growth substrate (SiO_2/Si with 200 nm Al seed layer) for the studies of mechanical transfer process. Since thermal annealing process enhances the crystalline quality of the material, we tried different annealing temperatures (350°C, 600°C, 800°C for 3 hr) for ZnO NWLs prior to the transfer process. It was observed that high annealing temperature tends to build strong bonding between ZnO NWLs and its growth substrate, making the exfoliation process challenging. Mechanical transfer of ZnO NWL with Tannealing >600°C causes significant damage to the film and consequently deteriorates the performance of the device. Thus, we identified that $T_{annealing} = 600°C$ is the optimum temperature of thermal annealing for transfer process. Figure 9a shows the photo image of the ZnO NWLs transferred to the Si substrate. The size of the transferred NWL film was 1.5 cm × 1.5 cm. Note that there were cracks on the transferred NWL film. These defects were caused by the scratching from the blade during the exfoliation process. As shown in the SEM image of Fig. 9b, the surface morphology of the ZnO NWLs was maintained after the transfer process.

To demonstrate the piezoelectricity of the transferred ZnO NWLs, we fabricated the prototype devices. Figure 10 shows the prototype device fabricated on flexible PI substrate. The voltage output

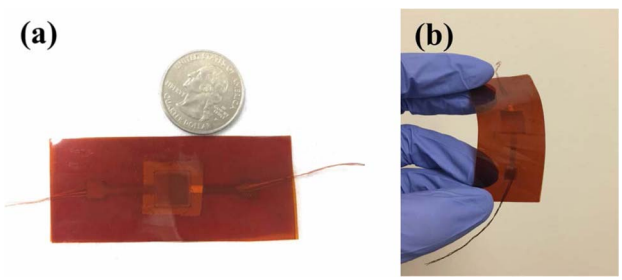

Figure 10. Photo image of (a) the ZnO NWL test device; and (b) bending of the device.

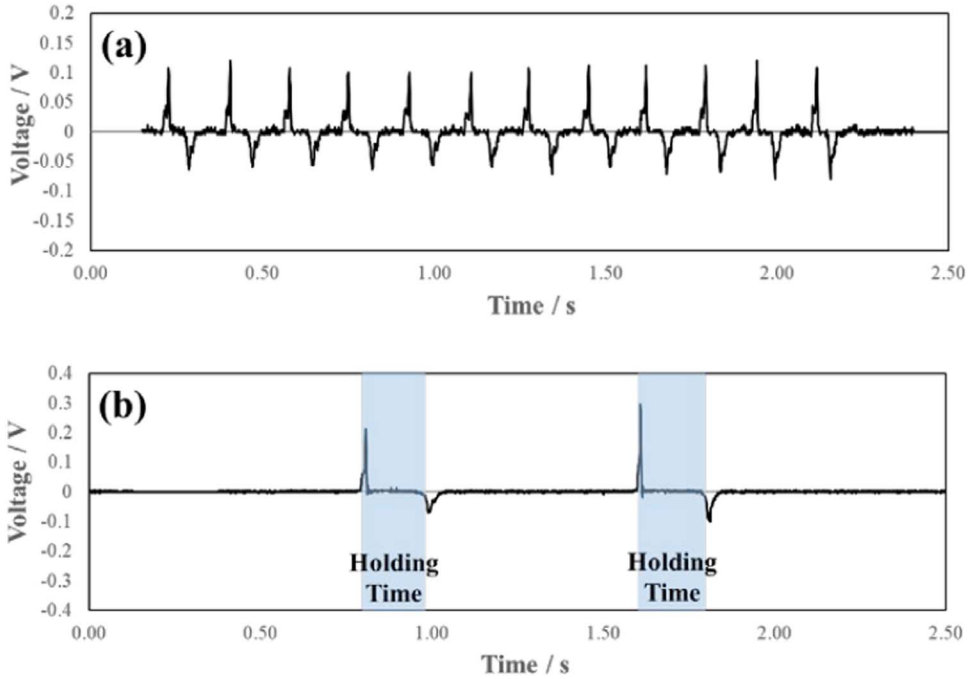

Figure 11. Recorded representative voltage-over-time log for a ZnO NWLs device with: (a) periodically applied pressure on device; (b) delayed release of pressure on device.

characteristic for a typical device is shown in Fig. 11a. As shown in the figure, pulse signals were generated with periodically applied finger force on top of the device. Fig. 11b plots the output signal as a function of time and with applied external force and delayed release. The positive output signal with applied force is from the compressive deformation of the ZnO NWLs, and the negative signal with the release of the external force is caused by material restoration. The maximum output voltage recorded was ~ 300 mV from the finger applied force. These devices showed similar output voltage characteristics as compared to the previously reported nanogenerators fabricated using ZnO nanorods[35–37] and ZnO nanowalls.[26,41] For the reference device with no NWLs embedded between the electrodes, no output voltage was observed.

To study the piezoelectric properties of the ZnO NWLs, COMSOL Multiphysics was used to develop a model with a honeycomb-like structure as shown in Fig. 12a. The simulated device is composed of ZnO hollow hexagon structure with electrodes at the top and bottom. Periodic boundary conditions were set on the sidewalls of the single hexagonal unit, sharing the boundary condition of deformation, elastic strain and electric potential with 6 neighboring hexagon units (see Supporting Information). Three geometric parameters were specified: nanowall height (h), nanowall lateral length (a), and nanowall thickness (t). In the simulation, the vertical pressure was applied on top of the device. The bottom electrode was fixed in position and electrically grounded. The potential difference between the top and bottom electrodes was calculated.

Based on the synthesized ZnO NWL structure, the following parameters were used in the simulation: a = 250 nm, t = 50 nm, h = 2.5 μm. These parameters were extracted from experimental characterization of the grown ZnO NWLs. From the simulation results, we observed that the voltage output is linearly proportional to both applied pressure and nanowall height. This is due to the deformation of ZnO NWLs in the vertical direction under applied force. A larger deformation builds up higher piezoelectric potential between the top and bottom electrodes. Fig. 12b plots the contour image of the electric potential of the hexagonal unit cell with the periodic boundary condition (see Supporting Information for details of the simulation). With an approximate 10 N of applied force and 0.5 cm × 0.5 cm contact

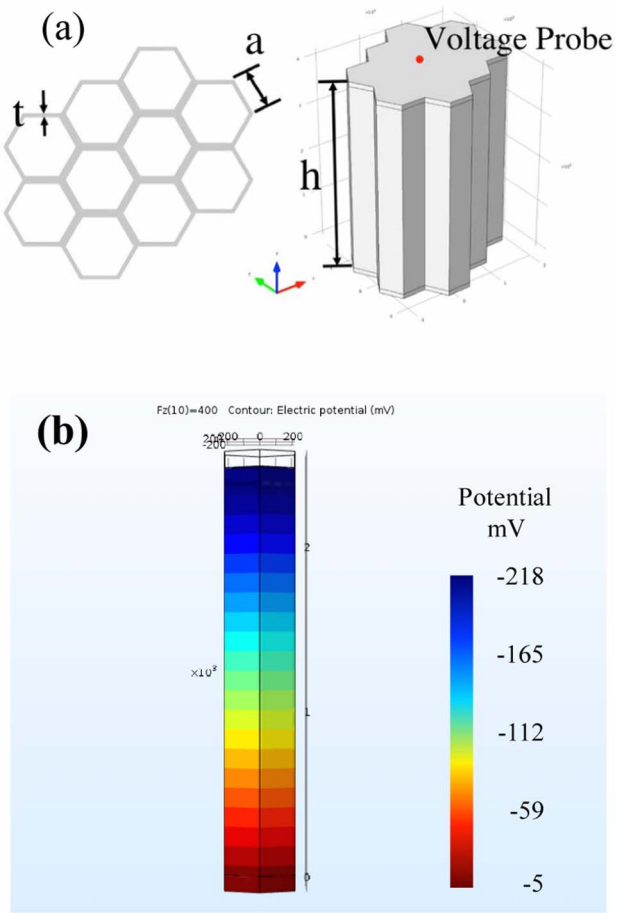

Figure 12. Modeling schematics of ZnO NWL in COMSOL Multiphysics. (a) tilted up hexagonal structures. (b) Electric potential contour plot of device with periodic boundary condition and applied external pressure of 400 kPa.

area during our device test, 400 kPa was estimated as the typical pressure applied to the devices under test. In the simulation, with the set pressure of 400 kPa, the corresponding output voltage is ∼210 mV. The simulation results are consistent with our experimental data.

Conclusions

In summary, we demonstrated the flexible prototype piezoelectric sensor device using the ZnO NWLs synthesized by hydrothermal process with aluminum as the seed layer. Comprehensive studies have been conducted to understand the effects of growth condition, seed layer thickness and thermal annealing process on material properties of ZnO NWLs. PMMA-medicated mechanical transfer process was used to transfer the as-grown ZnO NWLs to target substrates. Prototype piezoelectric ZnO NWLs sensor devices with a typical output voltage of 100 mV and maximum output voltage of 300 mV were fabricated. The experimental results match well with simulation. The developed transfer process is also applicable for various substrates with different active materials. Solution synthesis of high quality ZnO NWLs and the mechanical transfer process pave the way to achieve low cost and scalable flexible electronic and biomedical sensor devices.

Acknowledgments

The authors thank the funding support from the National Science Foundation (NSF-1664368).

ORCID

Hongping Zhao https://orcid.org/0000-0002-5169-5290

References

1. X. Wang, C. J. Summer, and Z. L. Wang, "Large-scale hexagonal-patterned growth of aligned ZnO nanorods for nano-optoelectronics and nanosensor arrays." *Nano Letters*, **4**(3), 423 (2004).
2. W. Water and S.-E Chen, "Using ZnO nanorods to enhance sensitivity of liquid," *Sensors and Actuators B: Chemical*, **136**(2), 371 (2009).
3. F. Xu and L. Sun, "Solution-derived ZnO nanostructures for photoanodes of dye-sensitized solar cells," *Energy Environ. Sci.*, **4**(3), 818 (2011).
4. Z.-L. Tseng, P.-C. Kao, M.-F. Shih, H.-H. Huang, J.-Y. Wang, and S.-Y. Chu, "Electrical bistability in hybrid ZnO nanorod/polymethylmethacrylate heterostructures," *Appl. Phys. Lett.*, **97**(21), 212103 (2010).
5. J. Wang, M. Xu, R. Zhao, and G. Chen, "A highly sensitive H_2O_2 sensor based on zinc oxide nanorod arrays film sensing interface," *Analyst*, **135**(8), 1992 (2010).
6. S. Bai, W. Wu, Y. Qin, N. Cui, D. J. Bayerl, and X. Wang, "High-Performance Integrated ZnO Nanowire UV Sensors on Rigid and Flexible Substrates," *Adv. Funct. Mater.*, **21**(23), 4464 (2011).
7. I.-H. Chan, J.-C. Chang, C.-T. Sun, M.-P. Houng, and S.-Y. Chu, "Deposition of Preferred-Orientation ZnO Films on the Lead-Free Ceramic Substrates and its Effects on the Properties of Surface Acoustic Wave Devices," *J. Am. Ceram. Soc.*, **95**(7), 2254 (2012).
8. H. Wan and H. E. Ruda, "A study of the growth mechanism of CVD-grown ZnO nanowires," *J. Mater. Sci. Mater. Electron.*, **21**(10), 1014 (2010).
9. M. H. Huang, Y. Wu, H. Feick, N. Tran, E. Weber, and P. Yang, "Catalytic Growth of Zinc Oxide Nanowires by Vapor Transport," *Adv. Mater.*, **13**(2), 113 (2001).
10. E. C. Greyson, Y. Babayan, and T. W. Odom, "Directed growth of ordered arrays of small diameter ZnO nanowires," *Adv. Mater.*, **16**(15), 1348 (2004).
11. Y. K. Tseng, H. C. Hsu, W. F. Hsieh, K. S. Liu, and I. C. Chen, "Two-step oxygen injection process for growing ZnO nanorods," *J. Mater. Res.*, **18**(12), 2837 (2003).
12. G. M. Kumar, P. Ilanchezhiyan, J. Kawakita, M. Subramanian, and R. Jayavel, "Magnetic and optical property studies on controlled low-temperature fabricated one-dimensional Cr doped ZnO nanorods," *Cryst. Eng. Commun.*, **12**(6), 1887 (2010).
13. M. M. Brewster, M.-Y. Lu, S. K. Lim, M. J. Smith, X. Zhou, and S. Gradecak, "The Growth and Optical Properties of ZnO Nanowalls," *J. Phys. Chem. Lett.*, **2**(15), 1940 (2011).
14. S.-W. Kim, S. Fujita, M.-S. Yi, and D. H. Yoon, "Catalyst-free synthesis of ZnO nanowall networks on Si_3N_4/Si substrates by metallorganic chemical vapor deposition," *Appl. Phys. Lett.*, **88**, 253114 (2006).
15. C.-H. Lee, Y.-J. Kim, J. Lee, Y. J. Hong, J.-M. Jeon, M. Kim, S. Hong, and G.-C. Yi, "Scalable network electrical devices using ZnO nanowalls," *Nanotechnol.*, **22**(5), 055205 (2011).
16. W. Z. Wang, B. Q. Zeng, J. Yang, B. Poudel, J. Y. Huang, M. J. Naughton, and Z. F. Ren, "Aligned Ultralong ZnO Nanobelts and Their Enhanced Field Emission," *Adv. Mater.*, **18**(24), 3275 (2006).
17. G. Z. Xing, X. S. Fang, Z. Zhang, D. D. Wang, X. Huang, J. Guo, L. Liao, Z. Zheng, H. R. Xu, T. Yu, Z. X. Shen, C. H. A. Huan, T. C. Sum, H. Zhang, and T. Wu, "Ultrathin single-crystal ZnO nanobelts: Ag-catalyzed growth and field emission property," *Nanotechnol.*, **21**(25), 255701 (2010).
18. M. Lucas, Z. L. Wang, and E. Riedo, "Growth direction and morphology of ZnO nanobelts revealed by combining in situ atomic force microscopy and polarized Raman spectroscopy," *Phys. Rev. B.*, **81**(4), 045415 (2010).
19. M. Wang, E. J. Kim, E. W. Shin, J. S. Chung, S. H. Hahn, and C. park, "Low-Temperature Solution Growth of High-Quality ZnO Thin Films and Solvent-Dependent Film Texture," *J. Phys. Chem. C*, **112**(6), 1920 (2008).
20. Y. Tak and K. Yong, "Controlled Growth of Well-Aligned ZnO Nanorod Array Using a Novel Solution Method," *J. Phys. Chem. B*, **109**(41), 19263 (2005).
21. Q. Ahsanulhaq, A. Umar, and Y. B. Hahn, "Growth of aligned ZnO nanorods and nanopencils on ZnO/Si in aqueous solution: growth mechanism and structural and optical properties," *Nanotechnol.*, **18**(11), 115603 (2007).
22. A. Orsini and C. FAlconi, "Real-time monitoring of the solution growth of ZnO nanorods arrays by quartz microbalances and in-situ temperature sensors," *Sci. Rep.*, **4**, 6285 (2014).
23. S. Bu, C. Cui, Q. Wang, and L. Bai, "Growth of ZnO Nanowires in Aqueous Solution by a Dissolution-Growth Mechanism," *J. Nanomater.*, **2008**, 610541 (2008).
24. S. Xu and Z. L. Wang, "One-Dimensional ZnO Nanostructures: Solution Growth and Functional Properties," *Nano Res.*, **4**(11), 1013 (2011).
25. S. A. Morin and S. Jin, "Screw Dislocation-Driven Epitaxial Solution Growth of ZnO Nanowires Seeded by Dislocations in GaN Substrates," *Nano Lett.*, **10**(9), 3459 (2010).
26. B. Saravanakumar and S.-J. Kim, "Growth of 2D ZnO Nanowall for Energy Harvesting Application," *J. Phys. Chem. C*, **118**(17), 8831 (2014).
27. Z. Liang, R. Gao, J. L. Lan, O. Wiranwetchayan, Q. Zhang, C. Li, and G. Cao, "Growth of vertically aligned ZnO nanowalls for inverted polymer solar cells," *Sol. Energy Mater. Sol. Cells*, **117**, 34 (2013).
28. N. Islavath, E. Ramasamy, D. Das, and S. V. Joshi, "Seed layer-assisted low temperature solution growth of 3D ZnO nanowall architecture for hybrid solar cells," *Mater. Des.*, **116**, 219 (2017).
29. A. Reina, X. Jia, J. Ho, D. Nezich, H. Son, V. Bulovic, M. S. Dresselhaus, and J. Kong, "Large area, few-layer graphene films on arbitrary substrates by chemical vapor deposition," *Nano letters*, **9**, 30 (2008).
30. L. Jiao, B. Fan, X. Xian, Z. Wu, J. Zhang, and Z. Liu, "Creation of Nanostructures with Poly(methyl methacrylate)-Mediated Nanotransfer Printing," *J. Am. Chem. Soc.*, **130**, 12612 (2008).
31. C. R. Dean, A. F. Young, I. Meric, C. Lee, L. Wang, S. Sorgenfrei, K. Watanabe, T. Taniguchi, P. Kim, K. L. Shepard, and J. Hone, "Boron nitride substrates for high-quality graphene electronics," *Nature Nanotechnology* **5**, 722 (2010).
32. J.-H. Ahn, H.-S. Kim, K. J. Lee, S. Jeon, S. J. Kang, Y. Sun, R. G. Nuzzo, and J. A. Rogers, "Heterogeneous Three-Dimensional Electronics by Use of Printed Semiconductor Nanomaterials," *Science*, **314**, 1754 (2006).
33. Y.-K. Chang and F. C.-N. Hong, "The fabrication of ZnO nanowire field-effect transistors by roll-transfer printing," *Nanotechnol.*, **20**(19), 195302 (2009).
34. K. Jenkins and R. Yang, "Mechanical transfer of ZnO nanowires for a flexible and conformal piezotronic strain sensor," *Semicond. Sci. Technol.*, **32**, 074004 (2017).
35. S.-H. Baek and I.-K. Park, "Flexible piezoelectric nanogenerators based on a transferred ZnO nanorod/Si micro-pillar array," *Nanotechnol.*, **28**(9), 095401 (2017).
36. Y. Hu, L. Lin, Y. Zhang, and Z. L. Wang, "Replacing a Battery by a Nanogenerator with 20 V Output," *Adv. Mater.*, **24**(1), 110. (2012).
37. S. Lee, R. Hinchet, Y. Lee, Y. Yang, Z.-H. Lin, G. Ardila, L. Montès, M. Mouis, and Z. L. Wang, "Ultrathin Nanogenerators as Self-Powered/Active Skin Sensors for Tracking Eye Ball Motion," *Adv. Funct. Mater.*, **24**(8), 1163 (2014).
38. J.-F. Tang, H.-H. Su, Y.-M. Lu, and S.-Y. Chu, "Controlled growth of ZnO nanoflowers on nanowall and nanorod networks via a hydrothermal method," *Cryst. Eng. Comm.*, **17**, 592 (2015).
39. H. Zhang, D. Yang, D. Li, X. Ma, S. Li, and D. Que, "Controllable Growth of ZnO Microcrystals by a Capping-Molecule-Assisted Hydrothermal Process," *Cryst. Growth Des.*, **5**, 547 (2005).
40. X.-G. Han, H.-Z. He, Q. Kuang, X. Zhou, X.-H. Zhang, T. Xu, Z.-X. Xie, and L.-S. Zheng, "Controlling Morphologies and Tuning the Related Properties of Nano/Microstructured ZnO Crystallites," *J. Phys. Chem. C*, **113**, 584 (2009).
41. A. A. Narasimulu, P. Zhao, N. Soin, K. Prashanthi, P. Ding, J. Chen, S. Dong, L. Chen, E. Zhou, C. D. Montemagno, and J. Luo, "Significant triboelectric enhancement using interfacial piezoelectric ZnO nanosheet layer," *Nano Energy*, **40**, 471 (2017).
42. H. Huang, H. Wang, B. Li, X. Mo, H. Long, Y. Li, H. Zhang, D. L. Carroll, and G. Fang, "Seedless synthesis of layered ZnO nanowall networks on Al substrate for white light electroluminescence," *Nanotechnol.*, **24**(31), 315203 (2013).
43. K. O. Iwu, V. Strano, A. Di Mauro, G. Impellizzeri, and S. Mirabella, "Enhanced Quality, Growth Kinetics, and Photocatalysis of ZnO Nanowalls Prepared by Chemical Bath Deposition," *Cryst. Growth Des.*, **15**, 4206 (2015).
44. Z. K. Tang, G. K. L. Wong, P. Y. Kawasaki, A. Ohtomo, and H. K. Segawa, "Room-temperature ultraviolet laser emission from self-assembled ZnO microcrystallite thin films," *Appl. Phys. Lett.*, **72**, 3270 (1998).
45. E. S. Shim, H. S. Kang, S. S. Pang, J. S. Kang, I. Yun, and S. Y. Lee, "Annealing effect on the structural and optical properties of ZnO thin film on InP," *Mater. Sci. Eng. B*, **102**, 366 (2003).
46. S. Y. Gao, H. D. Li, J. J. Yuan, Y. A. Li, X. X. Yang, and J. W. Liu, "ZnO nanorods/plates on Si substrate grown by low-temperature hydrothermal reaction," *Applied Surface Science*, **256**(9), 2781. (2010).